Tribology International 66 (2013) 125–133

Contents lists available at SciVerse ScienceDirect

Tribology International

journal homepage: www.elsevier.com/locate/triboint

# The lubricity of oil-in-water emulsion in cold strip rolling process under mixed lubrication

Sy-Wei Lo [a], Tzu-Chun Yang [b,*], Heng-Sheng Lin [c]

[a] Department of Mechanical Engineering, National Yunlin University of Science and Technology, Douliou City, Yunlin 64002, Taiwan
[b] Department of Mechanical Engineering, National Chin-Yi University of Technology, Taichung City 41170, Taiwan
[c] Department of Mold and Die Engineering, National Kaohsiung University of Applied Sciences, Kaohsiung City 80778, Taiwan^

ARTICLE INFO

*Article history:*
Received 5 November 2012
Received in revised form
22 March 2013
Accepted 17 April 2013
Available online 29 April 2013

*Keywords:*
Emulsion
Strip rolling
Phase inversion
Mixed lubrication

ABSTRACT

A mixed lubrication analysis of strip rolling has been developed to investigate the lubricity of oil-in-water emulsion. The combination of rolling speed and supply concentration determines the pattern of pressure distribution in the inlet zone. For emulsions of very low concentration, considerable hydrodynamic pressure still can be generated by transforming the emulsion into pure oil in the work zone; the lower concentration yields the higher peak of hydrodynamic pressure near the outlet. In addition to the rolling speed, the asperity adhesion is the dominant factor to augment the hydrodynamic pressure and the oil concentration by confining the lubricant flux with smaller film thickness. The bigger oil droplet, which plays the secondary role, also helps pressurize the lubricant.



## 1. Introduction

Usually metal strips possessing the final surface finishing must be fabricated via a rolling process in the mixed lubrication regime so that a preferred surface topography can be achieved. The contact mechanics of the asperity is simultaneously influenced by the bulk plastic flow of the strip and its interaction with the surrounding lubricant. This sophisticated process has been modeled by a number of researchers, mostly within Wilson's research group [1–4] for neat oil lubricant. Qiu et al. [5] released the strip from the constraint of a constant yield stress in mixed lubrication regime. Recently Lu et al. [6] studied the influence of the elastic deformation of the strip in the inlet zone on the inlet film thickness. All these efforts already shed light on the basic mechanisms of a rolling process lubricated with pure oil.

However, the oil-in-water (O/W) emulsion has become a common lubricant in strip rolling applications since compared with neat oil, it owns the advantages of cooling ability and cost saving. Numerous theoretical and experimental investigations have been tried to grip a full understanding of the complicated behaviors of emulsions, while to date it still remains a challenging task. Several experiments have been conducted to observe the two-phased lubrication, such as Nakahara et al. [7], Zhu et al. [8], and Yang et al. [9,10]. They concluded that the droplet size and initial oil concentration have a strong effect on the oil pool (particularly when the droplet sizes and concentration are below 5 μm and 5%, respectively, as pointed by Yang et al. [10]). At higher mean droplet sizes and concentrations, the influences of these variables are less significant. Beyond a certain critical speed, they found that the film thickness levels off quickly with increasing speed, more like a starved lubrication and at last water is entrained to form a water-like emulsion, resulting in unstable product surface and high consumption of electric power due to a hasty jump of both load and torque on the roller. This will change the product surface quality and will impose extra burdens on the rolling rig.

In addition to the physical factors such as the supply oil concentration, droplet size and the rolling speed, the chemical parameters like the emulsifier and the pH value of the surfactant solution also manipulate the amount of oil trapped in the roll bite entry. For instance, Cambiella et al. [11] used three different emulsifiers – anionic, nonionic and cationic – at different concentrations in the design of lubricant O/W emulsions. They pointed out that the interactions between metal and oil droplets rule the mechanism of lubrication and that this interaction is primarily controlled by emulsifier concentration. Azushima et al. [12] also carried out a series of cold rolling tests and confirmed that the plating-out film thickness increased with increasing emulsion concentration, and was relatively dependent on the affinity of the emulsion particle for the steel surface of the emulsifier.

In spite of the importance of chemical properties, several continuum models have been attempted, for example, by Al-Sharif et al. [13], Wang and Szeri [14], Dai and Khonsari [15], Szeri

* Corresponding author. Tel.: 886 4 23924505x7184; fax: 886 4 23930681.
*E-mail addresses:* losw@yuntech.edu.tw (S.-W. Lo), tcyang@ncut.edu.tw (T.-C. Yang), hslin@cc.kuas.edu.tw (H.-S. Lin).

0301-679X/$ - see front matter © 2013 Elsevier Ltd. All rights reserved.
http://dx.doi.org/10.1016/j.triboint.2013.04.018

**Nomenclature**

| | |
|---|---|
| $a_r$ | roll radius |
| $A$ | fractional contact area |
| $A^*$ | dimensionless roll radius |
| $c_a$ | adhesion coefficient |
| $C$ | constant of integration |
| $d$ | droplet diameter |
| $D$ | dimensionless droplet diameter |
| $E$ | dimensionless bulk strain rate |
| $f_1, f_2$ | functions of fractional contact area |
| $h$ | nominal surface separation |
| $h_t$ | surface gap (average film thickness) |
| $h_{t1}$ | surface gap at inlet-work boundary |
| $H$ | dimensionless nominal surface separation |
| $H_t$ | dimensionless surface gap (average film thickness) |
| $H_{t1}$ | dimensionless surface gap at inlet-work boundary |
| $H_{t2}$ | dimensionless surface gap at work-outlet boundary |
| $K$ | coefficient of wall (solid surface) effect |
| $L$ | asperity half pitch |
| $L^*$ | dimensionless asperity half pitch |
| $m$ | friction factor |
| $m_f$ | dimensionless shear strength of bulk lubricant |
| $M$ | dimensionless effective viscosity |
| $p$ | average interface pressure |
| $p_c$ | pressure of continuous phase |
| $p_d$ | pressure of disperse phase |
| $p_f$ | fluid (hydrodynamic) pressure |
| $p_{oil}$ | oil pressure |
| $P$ | dimensionless average interface pressure |
| $P_f$ | dimensionless fluid (hydrodynamic) pressure |
| $R$ | reduction |
| $R^*$ | dimensionless roughness |
| $R_h$ | dimensionless reciprocal film thickness |
| $R_q$ | composite surface roughness |
| $S$ | dimensionless rolling speed |
| $T_b$ | dimensionless back tension on strip |
| $T_f$ | dimensionless front tension on strip |
| $u_r$ | surface speed of roll |
| $u_s$ | surface speed of strip |
| $u_1$ | inlet speed of strip |
| $u_2$ | outlet speed of strip |
| $U_r$ | dimensionless roller speed |
| $U_s$ | dimensionless strip speed |
| $x$ | coordinate with origin on the center line of the rollers |
| $x'$ | distance from the virtual intersection of the strip and roll surfaces |
| $x_1$ | distance from inlet-work boundary |
| $x_i$ | distance from the start of inlet zone |
| $x_o$ | distance from the end of outlet zone |
| $X$ | dimensionless coordinate for work and outlet zone analysis |
| $X'$ | dimensionless coordinate for inlet zone analysis |
| $y$ | strip local thickness |
| $y_1$ | original thickness of strip |
| $y_2$ | thickness of rolled strip |
| $Y$ | dimensionless local strip thickness |
| $Z$ | outlet speed ratio |
| $\alpha_c$ | fraction of pressure of continuous phase |
| $\alpha_d$ | fraction of pressure of disperse phase |
| $\beta_c$ | fraction of pressure gradient of continuous phase |
| $\beta_d$ | fraction of pressure gradient of disperse phase |
| $\gamma$ | pressure coefficient of viscosity |
| $\eta$ | (dynamic) viscosity |
| $\eta_o$ | viscosity of oil at ambient pressure |
| $\eta_{oil}, \eta_{water}$ | viscosities of oil and water, respectively |
| $\lambda$ | viscosity ratio of oil to water |
| $\mu$ | effective viscosity of emulsion |
| $\xi$ | equivalent viscosity of emulsion |
| $\theta_a$ | asperity slope |
| $\sigma_Y$ | yield stress of strip |
| $\phi$ | volume fraction |
| $\phi_{inv}$ | volume fraction of disperse phase at inversion |
| $\phi^*$ | normalization factor for viscosity of emulsion |
| $\Phi_p$ | pressure flow factor |
| $\Omega$ | dimensionless equivalent viscosity |

*Subscripts*

| | |
|---|---|
| $c$ | continuous phase |
| $d$ | disperse phase |

and Wang [16], and Yan and Kuroda [17,18]. On the other hand, Wilson et al. [19,20] proposed that the dynamic concentration of oil starts in the roll bite entry only when the gap becomes some fraction of the oil droplet diameter. A model similar to the starved lubrication for pure oil was accordingly introduced. All these models and their hybrid types have been applied to rolling problems. For instance, Cassarini et al. [21] and Montmittonet et al. [22] combined the continuum model of Wang and Szeri [14] with Wilson's dynamic theory to match the rolling experiments under realistic semi-industrial conditions. Kosasih and Tieu [23] adopted Yan and Kuroda's [17,18] concept of the equivalent viscosity for thin-film regime to treat the low-speed, high concentration strip rolling. Tieu et al. [24] also extend their study to analyze the thermal distributions in roll and strip. Benner et al. [25] studied the effect of water as a contaminant in lubricated contacts using the theory of Al-Sharif et al. [13]. They concluded that for heavily loaded contacts water-in-oil emulsions perform essentially the same as pure oils.

Recently, Lo et al. [26] developed an emulsion theorem which is able to model the transition from thick to thin film regions, including the wall (solid surface) effect. The relationships concerning the pressures and the pressure gradients of the two phases have been derived based on the results from a series of CFD simulations. The condition in the inception of inversion is also proposed. Lo et al. used this model to simulate a simple 2D cylinder-plane rolling system and compared the calculated film thickness with the measured one. The results are generally in accordance with the experiment over a broad range of rolling speed [1]. In the following section, the emulsion model will be joined with a plasticity analysis to comprehend the lubricity of O/W emulsions used in a strip rolling process.

## 2. Strip rolling system

The geometry of the process to be analyzed is shown in Fig. 1. A strip of original thickness $y_1$ is rolled through a pair of rolls with radius $a_r$ to get the final thickness $y_2$. It is assumed that the rolls and the strip have longitudinal roughness lay. The emulsion generally having volume fraction below 5% of mineral or synthetic oil is provided near the entry to the roll bite. The strip in process is divided into three sections, namely, the inlet, work, and outlet

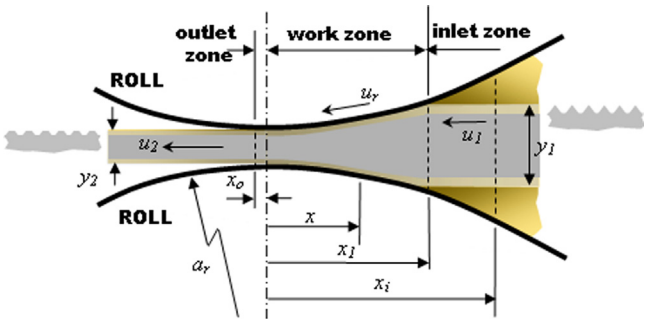


**Fig. 1.** System to be analyzed.

zones respectively to facilitate the lubrication analysis. In the inlet zone, the strip is considered as rigid and both the concentration and pressure of the emulsion build up rapidly to yield the strip at the inlet-work boundary. The strip undergoes plastic deformation in the work zone and regains rigidity at the plane of the roll axes where the hydrodynamic pressure between roll and strip begins to drop fast and returns to zero at the end of the outlet zone.

## 3. Theoretical model

Considering the steady rolling process of strips with longitudinal roughness, we may modify the Reynolds equation of Lo et al. [26] for the hydrodynamic pressure $p_f$ as:

$$dp_f/dx = (\xi/\Phi_p h_t^3)[c-6(u_r+u_s)h_t] \quad (1)$$

where $\xi$ is the equivalent viscosity, $u_r$ is the roller speed, $u_s$ is the strip speed, $\Phi_p$ is the pressure flow factor describing the influence of the surface roughness on the flux of pressure flow, $h_t$ is the surface gap (average film thickness), and $c$ is the constant of integration. The hydrodynamic pressure is composed of pressures from different phases and

$$p_d = \alpha_d p_f \quad (2)$$

$$p_c = \alpha_c p_f \quad (3)$$

where $\alpha_d$ and $\alpha_c$ are the fractions of pressures for the dispersed phase and the continuous phase, respectively. The equivalent viscosity $\xi$ is defined by:

$$\frac{1}{\xi} = \frac{\phi_d}{\xi_d} + \frac{\phi_c}{\xi_c} \quad (4)$$

where $\phi_d$ and $\phi_c$ are the volume fractions and the equivalent viscosities for the two phases are:

$$\xi_d = \frac{\mu_d\mu_c - \mu_{dc}\mu_{cd}}{\beta_d\mu_c - \beta_c\mu_{dc}} \quad (5)$$

$$\xi_c = \frac{\mu_d\mu_c - \mu_{dc}\mu_{cd}}{\beta_c\mu_d - \beta_d\mu_{cd}} \quad (6)$$

The viscosity coefficients $\mu$, $\mu B_d$, $\mu B_c$, $\mu B_{dc}$, and $\mu B_{cd}$ are related to the effects of the shear rates on the shear stresses as the emulsion is assumed Newtonian, and

$$\beta_d = \phi_d\alpha_d \quad (7)$$

$$\beta_c = \phi_c\alpha_c \quad (8)$$

$$\beta_d + \beta_c = 1 \quad (9)$$

All the viscosity coefficients and the different definitions of viscosity are summarized in Table 1. In Table 1, $\eta_d$ and $\eta_c$ are the viscosities of the mediums in their pure states, respectively. It is notable that in the beginning, the oil plays the role of the disperse medium in an O/W emulsion. But it will become the continuous one after inversion. Another function $K$, the coefficient of wall effect, in Table 1 represents the influence from the solid walls on the fluid viscosities, ranging from thick-film to thin-film regime, is related to the ratio of the surface gap $h_t$ to the oil droplet diameter $d$

$$h_t/d = H_t/D \quad (10)$$

where

$$H_t = h_t/R_q \quad (11)$$

$$D = d/R_q \quad (12)$$

are the dimensionless surface gap and dimensionless droplet diameter, respectively; while $R_q$ represents the composite surface roughness of the roll and the strip. The effect of solid walls on the emulsion fades away as the ratio $H_t/D$ approaches 10. On the other hand, the droplet will convert into an oil bar (column) connecting the adjacent solid surfaces when the film thickness becomes sufficiently small (set as 0.8 of the droplet diameter in the model). Since the function $K$ is not rigorously determined, the other smooth and reasonable functions might be also acceptable. To both simplify the analysis and avoid any influence from the choice of function $K$, we will use only the two formulations for thick and thin films, respectively, in our following calculation.

A series of numerical simulations have been conducted by Lo et al. [26] to investigate the pressure ratio $\alpha_d$ and the following form is proposed:

$$\alpha_d = p_d/p_f = 1 + (1-\phi_d/\phi_{inv})^2[1-\exp(-0.168H_t/D)] \quad (13)$$

where $\phi_{inv}$ is the volume fraction at inversion. It is well known that inversion will occur when the volume fraction of the dispersed phase is about 0.7. Based on the considerations of the flow impedance and the medium viscosity, the volume fraction at inversion, $\phi_{inv}$, is given as [26]:

$$\phi_{inv} = (0.0424\ln\lambda + 1.299)[\phi^* - 1.350\exp(-0.683\ln\lambda)] \quad (14)$$

The parameter $\phi^*$, usually shifting between 0.4 and 0.5, accounts for factors inherent in the emulsion that affect the viscosity, such as type of emulsifier, droplet size, and the shear rate. The parameter $\lambda$ is the ratio of oil viscosity to water viscosity:

$$\lambda = \eta_{oil}/\eta_{water} \quad (15)$$

We also assume that only the oil viscosity varies according to the Barus law:

$$\eta_{oil} = \eta_o \exp(\gamma p_{oil}) \quad (16)$$

**Table 1**
Summary of viscosity coefficients [26].

| | Before inversion | After inversion |
|---|---|---|
| Thick zone ($H\to\infty$) | $\mu_d = \phi_d^4\eta_d + \mu_{m\infty}$<br>$\mu_c = \phi_c\eta_c + \mu_{m\infty}$<br>$\mu_{dc} = \mu_{cd} = \mu_{m\infty}$<br>$= (\mu_\infty - \phi_d^4\eta_d - \phi_c\eta_c)/4$ | $\mu_d = \phi_d^4\eta_d + \mu_{m\infty}$<br>$\mu_c = \phi_c\eta_c + \mu_{m\infty}$<br>$\mu_{dc} = \mu_{cd} = \mu_{m\infty}$<br>$= (\phi_d - \phi_d^4)\eta_d/4$ |
| | $\mu_\infty = \frac{\eta_c}{(1-0.60\phi_d/\phi^*)^{2.5}}$ | $\mu_\infty = \phi_d\eta_d + \phi_c\eta_c$ |
| Thin zone ($H\le 0.8$) | $\mu_d = \phi_d\eta_d$<br>$\mu_c = \phi_c\eta_c$<br>$\mu_{dc} = \mu_{cd} = \mu_m = 0$<br>$\mu_0 = \phi_d\eta_d + \phi_c\eta_c$ | $\mu_d = \phi_d\eta_d$<br>$\mu_c = \phi_c\eta_c$<br>$\mu_{dc} = \mu_{cd} = \mu_m = 0$<br>$\mu_0 = \phi_d\eta_d + \phi_c\eta_c$ |
| General form | $\mu_c = \phi_c\eta_c + \mu_m$<br>$\mu_d = \mu - 3\mu_m - \phi_c\eta_c$<br>$\mu = \mu_0 - K(\mu_0 - \mu_\infty)$<br>$\mu_m = K\mu_{m\infty} = K(\mu_\infty - \phi_d^4\eta_d - \phi_c\eta_c)/4$<br>$K = 1-\exp[(0.8-H_t/D)/2]$ for $H_t/D > 0.8$<br>$K = 0$ for $H_t/D \le 0.8$ | |

where $\eta_o$ is the oil viscosity at zero (ambient) pressure and $\gamma$ is the pressure coefficient.

According to Lo et al. [26], two equations of conservation can be derived to calculate the volume fractions of disperse and continuous phases at different locations:

$$\phi_d\{H_t(1+U_s)+(\Omega/\Omega_d)[C/6S-(1+U_s)H_t]\}=C_d \tag{17}$$

$$\phi_c\{H_t(1+U_s)+(\Omega/\Omega_c)[C/6S-(1+U_s)H_t]\}=C_c \tag{18}$$

where the dimensionless equivalent viscosities are defined by

$$\Omega=\xi/\eta_o;\ \Omega_d=\xi_d/\eta_o;\ \Omega_c=\xi_c/\eta_o \tag{19}$$

The dimensionless surface speed of strip $U_s$ is a function of the dimensionless local strip thickness $Y$:

$$U_s=u_s/u_r=Z(1-R)/Y \tag{20}$$

$$Y=y/y_1 \tag{21}$$

and

$$R=(y_1-y_2)/y_1 \tag{22}$$

$$Z=u_2/u_r \tag{23}$$

are the reduction and the outlet speed ratios, respectively. It can be seen that $Y=1$ and $Y=(1-R)$ are for inlet and outlet zones. The two constants $C_d$ and $C_c$ are calculated by the "supply" properties of emulsion in the far upper stream of the inlet zone.

### 3.1. Inlet zone

In the inlet zone (IZ), the nominal surface separation $h$ is given approximately by

$$h=x'x_1/a_r \tag{24}$$

where $x'$ is the distance from the virtual intersection of the incoming strip and roll surfaces, $x_1$ is the distance from the inlet-work boundary to the plane joining roll centers and $a_r$ is the roll radius. The dimensionless nominal surface separation $H$ is therefore defined by

$$H=h/R_q \tag{25}$$

Adopting a simplified pattern of longitudinal serrated roughness of Chang et al. [3], we have

$$\begin{aligned} &H_t=H;\ \Phi_P=1+3/{H_t}^2 \text{ for full-film region } (H_t\geqq\sqrt{3})\\ &H_t=(H+\sqrt{3})^2/4\sqrt{3};\ \Phi_P=2\sqrt{3}/H_t \text{ for mixed region } (\sqrt{3}>H_t>0)\end{aligned} \tag{26}$$

The Reynolds equation can be rewritten in the dimensionless form:

$$dP_f/dX'=(\Omega/\Phi_P{H_t}^3)\{C-6S[1_B+Z(1-R)]H_t\} \tag{27}$$

where

$$P_f=p_f/\sigma_Y \tag{28}$$

$$X'=x'x_1/a_rR_q \tag{29}$$

$$S=\eta_o a_r u_r/\sigma_Y R_q x_1 \tag{30}$$

are the dimensionless hydrodynamic pressure, dimensionless position in the inlet zone and dimensionless speed respectively; while $\sigma_Y$ is the yield stress of the strip. Since in the full film region, the three variables $X'$, $H$, and $H_t$ are identical, we may follow the approach of Lin et al. [4] to facilitate the integration of Eq. (27) by using the dimensionless reciprocal film thickness $R_h$:

$$R_h=1/H_t \tag{31}$$

Thus, the dimensionless Reynolds equation becomes

$$dP_f/dR_h=(\Omega/\Phi_p)\{6S[1_B+Z(1-R)]-CR_h\} \tag{32}$$

Eq. (32) can be integrated numerically with respect to the boundary condition:

$$P_f=0 \text{ at } R_h=0 \tag{33}$$

to get the dimensionless hydrodynamic pressure until asperity contact happens, that is

$$P_f=P_{fc} \text{ at } R_h=1/\sqrt{3} \tag{34}$$

In the mixed region of the inlet zone, despite that asperity contact shares part of the load, the bulk strip remains rigid and thereby the relation $H=X'$ holds. Eq. (26) is used to transform $H$ into $H_t$ due to asperity deformation. The Reynolds equation is thus expressed as:

$$dP_f/dH_t=\frac{1.316\Omega}{\Phi_p H_t^3\sqrt{H_t}}\{C-6S[1_B+Z(1-R)]H_t\} \tag{35}$$

The above equation is integrated from the onset of asperity contact ($H_t=\sqrt{3}$) with $P_f=P_{fc}$ to get $H_t=H_{t1}$ and $P_f=P_{f1}$ at the inlet-work boundary, which have to satisfy the following conditions:

$$P_{f1}=1-T_b-A/f_2(A) \tag{36}$$

where

$$T_b=\sigma_b/\sigma_Y \tag{37}$$

is the dimensionless back tension on the strip, $\sigma_b$ is the back tension on the strip, $A$ is the fractional contact area, and $f_2$ is the function given by Sheu and Wilson [1]. For serrated roughness, the fractional contact area and the dimensionless surface gap are related geometrically by

$$A=1-[H_t/\sqrt{3}]^{1/2} \tag{38}$$

As for the constants $C_d$ and $C_c$ for concentration calculations, we may assume that the concentration happens when the average surface gap is smaller than, either 10 times of the surface roughness so that the roughness disturbance can be neglected, or 10 times of the oil droplet diameter so that the wall effect can be ignored. This seems somewhat similar to the dynamic concentration model of Wilson et al. [19]. However, the extremity of concentration area is coupled with droplet diameter. With this in mind, we suggest that Eqs. (17) and (18) are activated at $H_{ti}$ (or $R_{hi}$) where

$$H_{ti}=\max[10,\ 10D] \tag{39}$$

or

$$R_{hi}=\min[1/10,\ 1/10D] \tag{40}$$

The two constants $C_d$ and $C_c$ are calculated using the data at this initial point. The initial (supply) oil concentration $\phi_d$ is denoted as $\phi_s$ and in the following downstream area, the oil and water concentrations are thus determined by Eqs. (17) and (18).

### 3.2. Work zone

In the work zone (WZ), the dimensionless Reynolds equation and the dimensionless equilibrium equations are written as

$$\frac{dP_f}{dX}=\frac{\Omega R}{R^*\Phi_p H_t^3}\{C-6S[1+Z(1-R)/Y]H_t\} \tag{41}$$

$$dP/dX=(2RX+m\sqrt{RA^*})/Y \tag{42}$$

where

$$X=x/x_1 \tag{43}$$

$$Y=1-R+RX^2 \tag{44}$$

$$A^*=a_r/y_1 \tag{45}$$

$$R^* = R_q/y_1 \tag{46}$$

$$P = p/\sigma_Y \tag{47}$$

$$M = \frac{2\mu u_r}{\sigma_Y R_q} \tag{48}$$

$$m_f = M[Z(1-R)/Y-1]/H_t \leqq c_a \tag{49}$$

and

$$m = Ac_a \ \mathrm{sign}[Z(1-R)/Y-1] + (1-A)m_f \tag{50}$$

are the dimensionless position, the dimensionless local strip thickness, the dimensionless roll radius, the dimensionless roughness, the dimensionless average interface pressure, the dimensionless effective viscosity, and the dimensionless shear strength of bulk lubricant and friction factor, respectively. The adhesion coefficient $c_a$ on asperity peaks is assumed constant and the expression of the effective viscosity $\mu$ is listed in Table 1. Notice that the shear strength of the bulk lubricant is assumed to be no greater than that of the boundary film, as proposed by Lin et al. [4], and we will truncate the calculated $m_f$ at a value of $c_a$.

The variations of the fractional contact area and the dimensionless strain rate will follow the model developed by Kosasih and Tieu [23]:

$$\mathrm{d}A/\mathrm{d}X = -2XR/\{\theta_a[2L^*(1-A) + YE]\} \tag{51}$$

$$E = [A/(P-P_f)-f_2]/f_1 \tag{52}$$

$$L^* = L/y_1 \tag{53}$$

where $\theta_a$ is the asperity slope, $E$ is the dimensionless bulk strain rate, $f_1$ is the function given by Sheu and Wilson [1], and $L$ is the asperity half pitch, respectively. Eqs. (41), (42) and (51) are integrated simultaneously from $X=1$ with the final results of the inlet zone analysis to the end of the work zone $X=0$. At the end of the work zone, the dimensionless pressure $P$ must fulfill the following condition:

$$P = 1-T_f \tag{54}$$

and

$$T_f = \sigma_f/\sigma_Y \tag{55}$$

is the dimensionless front tension on the strip. The final $H_t$ at the end of the work zone is denoted as $H_{t2}$. The model can be extended to the "high-speed" mixed lubrication as that proposed by Lin et al. [4].

### 3.3. Outlet zone

In the outlet zone (OZ), the same dimensionless Reynolds equation as that for work zone analysis is used with $Y=(1-R)$ and the dimensionless surface gap is described by

$$H_t = H_{t2} + RX^2/2R^* \tag{56}$$

The lubricant pressure drops fast in the diverging surface gap between roll and rigid strip. Since at the end of the outlet zone $X_o$, both the hydrodynamic pressure and the pressure gradient turn into zero, we can integrate the lubricant pressure from $X=0$ until the pressure gradient $\mathrm{d}P_f/\mathrm{d}X$ vanishes and $P_f$ must satisfy the condition:

$$P_f = 0 \text{ at } X = X_o \tag{57}$$

A double shooting technique similar to that of Lin et al. [4] is used by adjusting $C$ and $Z$ to fulfill the boundary conditions Eq. (54) for $P$ at the end of work zone and Eq. (57) for $P_f$ at the end of the outlet zone.

## 4. Results and discussion

The flow chart of the solving procedures is shown in Fig. 2. Fig. 3 shows the variations of the hydrodynamic pressure for four supply oil concentrations, or called the initial oil concentration, $\phi_s$ (1–5%) and two dimensionless speeds (0.01, 0.001). The dimensionless droplet diameter $D$ is equal to unity and the friction factor $c_a$ is set as 0.2, which is common for many metal strips. In the inlet zone, the hydrodynamic pressure is dominated by the dimensionless speed. For dimensionless speed $S$ equals 0.001, only the emulsion with higher concentration like 3% and 5% can be effectively pressurized. Their pressures suddenly climb up around the dimensionless position $X=1.001$ where the surface gap is small enough for the oil droplet to "bridge" the surfaces and becomes an oil column. This is the situation presumed in Wilson's dynamic concentration model [19] that a distinct pressuring zone

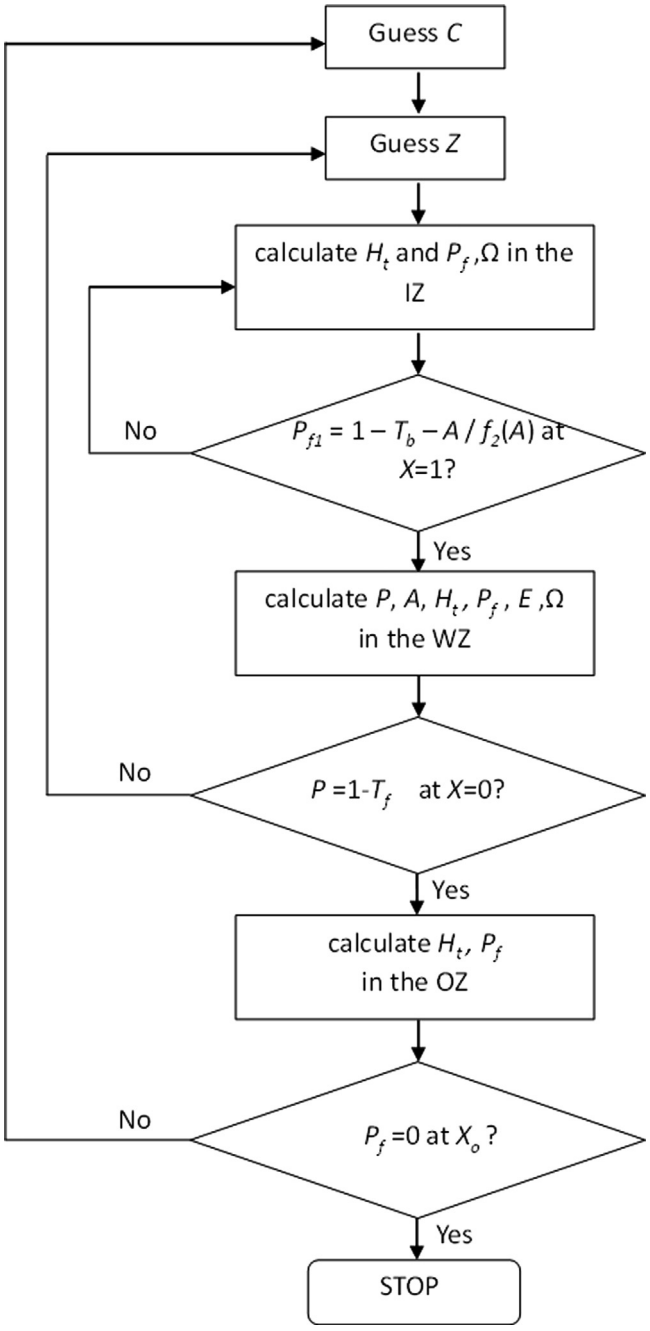


**Fig. 2.** Flow chart of solving procedures.

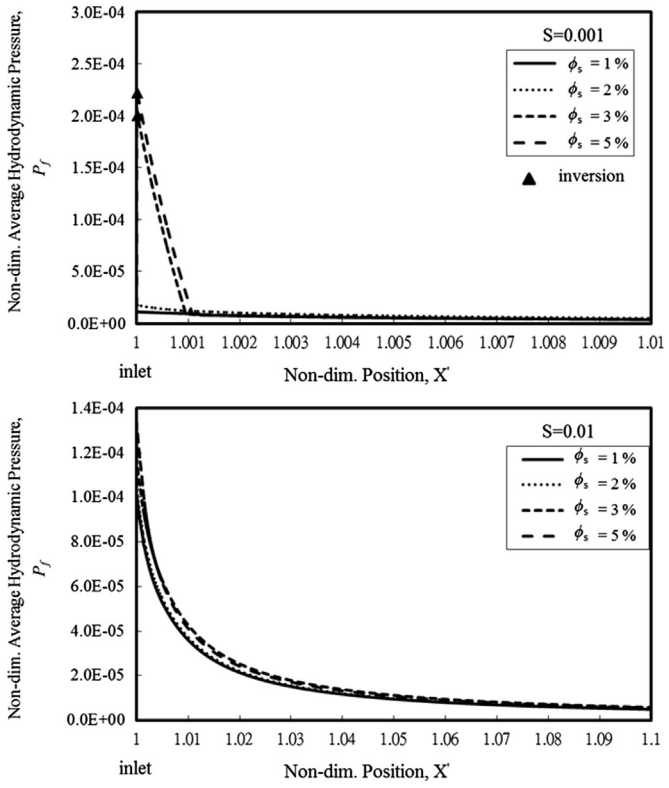


**Fig. 3.** Average hydrodynamic pressure in the inlet zone.

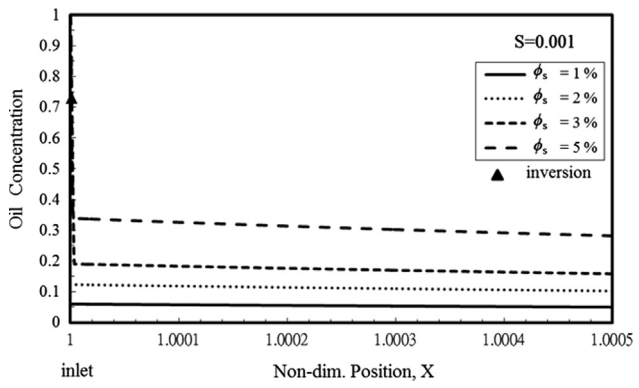


**Fig. 4.** Concentration of the disperse phase in the inlet zone.

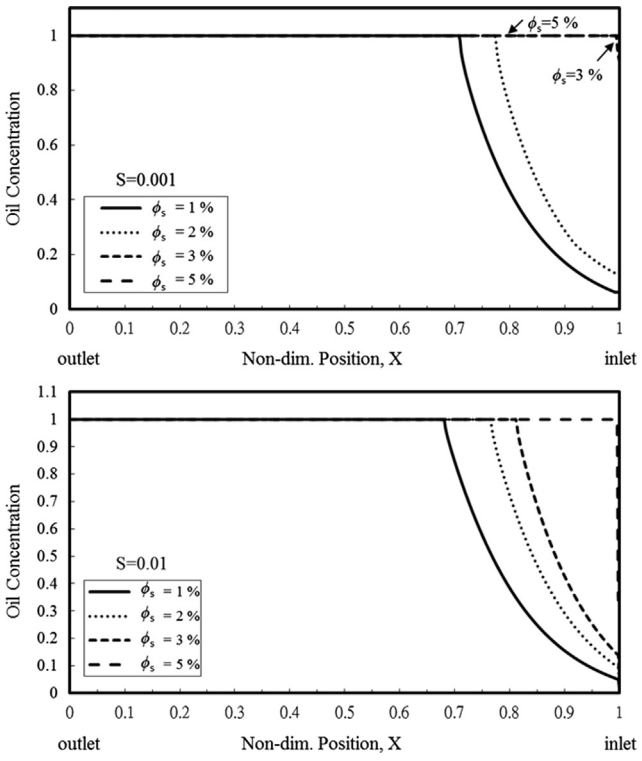


**Fig. 5.** Concentration of the disperse phase in the work zone.

can be defined. On the contrary, the higher speed $S=0.01$ brings on smooth curves and the final pressures at the end of the inlet zone are lower than that of $S=0.001$. Such a lower hydrodynamic pressure in the high speed case is irrelevant to the degree of asperity flattening since the changes in the fractional contact area $A$ and the film thickness $H_t$ for $S=0.001$ and $S=0.01$ are almost identical. Fig. 4 shows that the combination of low speed and high concentration can increase the viscosity, which eventually has the opportunity to induce the phase inversion accompanied with better hydrodynamic pressure. On the other hand, it is well known from experimental observations that enhancing the rolling speed will bring more water into the roll bite and dilute the emulsion. Fig. 5 theoretically verifies this by showing that the greatest final concentration at the inlet/work zone boundary is only about 35% when S=0.01, much less than the threshold for inversion.

Fig. 5 shows that in the upper stream area of the work zone, all the O/W emulsions will eventually transform into the W/O state and become pure oil rapidly, due to the difference between oil and water speeds, as explained by Yan and Kuroda [17,18]. The hydrodynamic pressure thus rises swiftly, as shown in Fig. 6 where the positions where inversion occurs are marked with a triangle symbol. Our simulation suggests that emulsions of supply concentration 5% can inverse in the inlet zone, generating a smooth variation of the hydrodynamic pressure. However, the curves for the lower concentrations are relatively sharp with greater peak values shifted toward the outlet. Fig. 6(a) also plots the hydrodynamic pressure calculated by Kosasih and Tieu [23] for 5% concentration with $S=0.001$. In spite of the comparable peak value, Kosasih and Tieu's result is generally lower than the present prediction, probably due to the ignorance of the pressure built up in the upper stream area of the inlet zone, as well as to the formulations of thin-film viscosities. The delayed-action inversion also forces the surface roughness to flatten, as can be observed from Fig. 7 for the fractional contact area.

In spite of the discrepancies mentioned above, the total interfacial pressure between roll and workpiece does not vary dramatically (shown in Fig. 8). Basically it falls only when the supply oil concentration and the dimensionless rolling speed are sufficiently high.

The influences of the dimensionless droplet diameter $D$ and the adhesion coefficient $c_a$ are investigated. Figs. 9–11 imply that the adhesion coefficient is the dominant factor to augment the hydrodynamic pressure and the oil concentrations. Fig. 12 indicates that the greater adhesion raises the average interface pressure in the work zone, due to the friction hill effect. The bigger oil droplet, which plays the secondary role, also helps pressurize the lubricant. The greater adhesion helps generate the hydrodynamic effect by flattening the asperities in the "work" zone (see Fig. 13), while the larger oil droplets can build up more hydrodynamic pressure in the "inlet" zone. The two mechanisms are coupled via the flux of the lubricant, which is related to the constant $C$ of the model. A high adhesion coefficient like 0.5 creates a very thin film, which

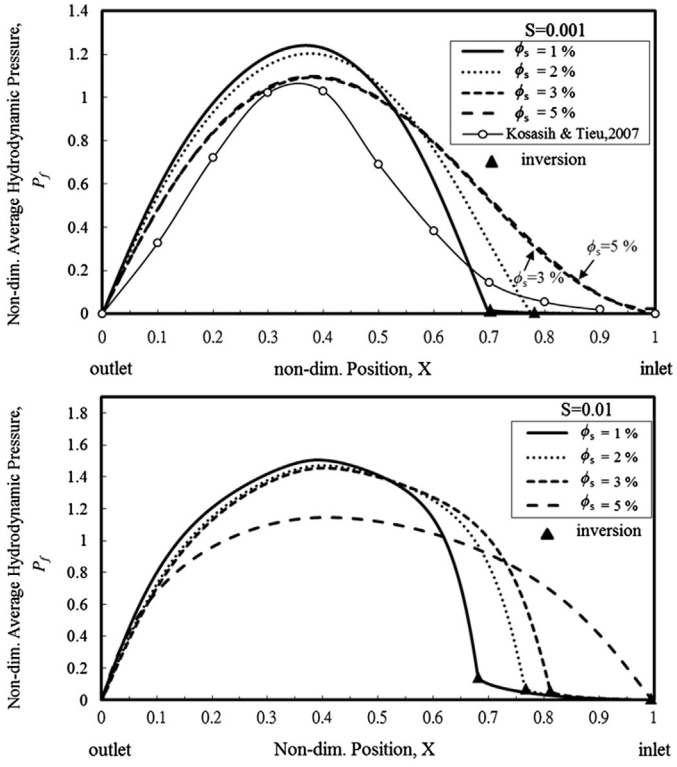


**Fig. 6.** Average hydrodynamic pressure in the work zone.

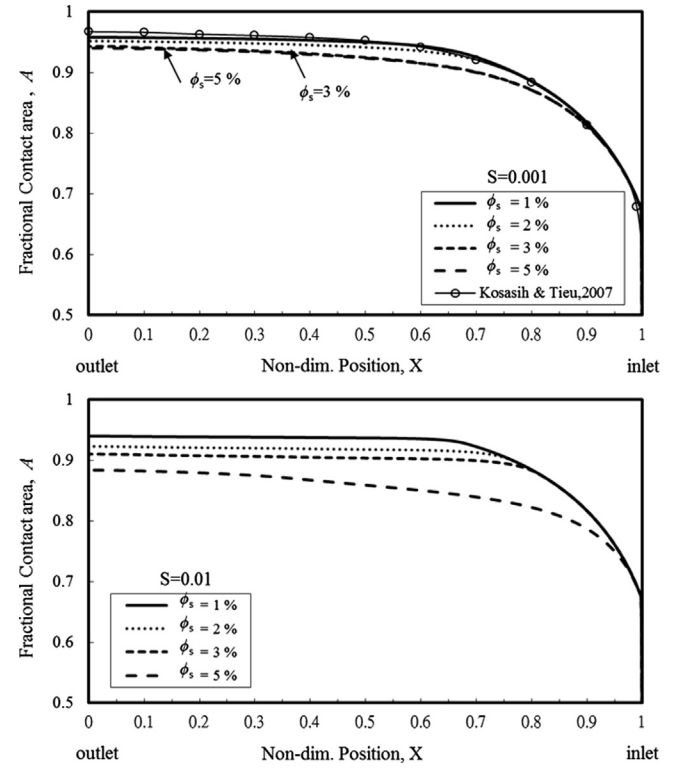


**Fig. 7.** Fractional contact area in the work zone.

results in high fluid pressure and low lubricant flux. The secondary effect from the droplet size in the inlet zone is therefore neglected.

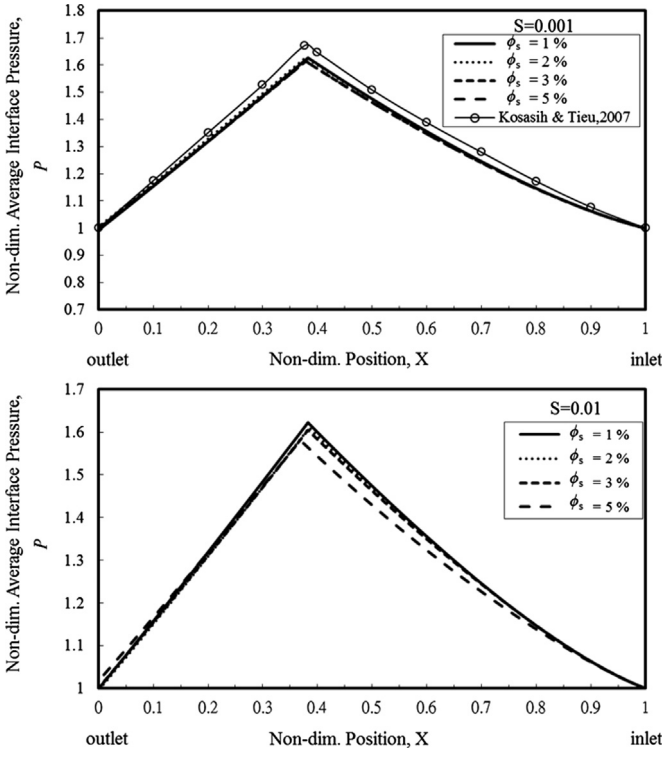


**Fig. 8.** Average interface pressure in the work zone.

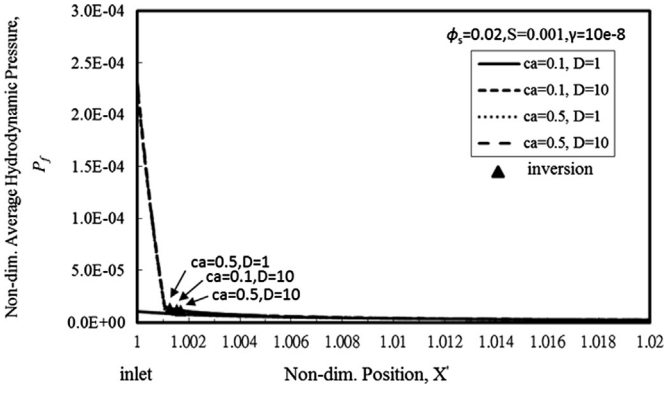


**Fig. 9.** Influences of droplet diameter and adhesion coefficient on hydrodynamic pressure in inlet zone.

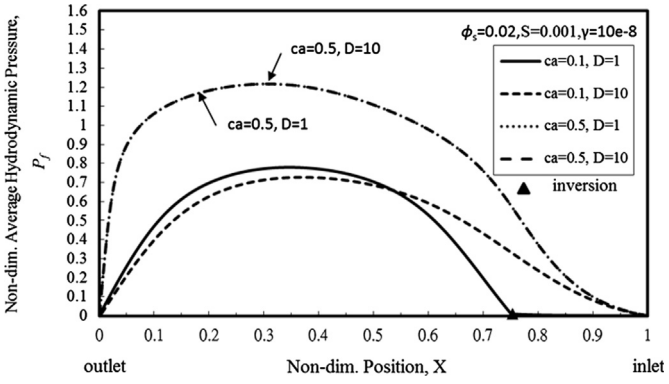


**Fig. 10.** Influences of droplet diameter and adhesion coefficient on hydrodynamic pressure in work zone.

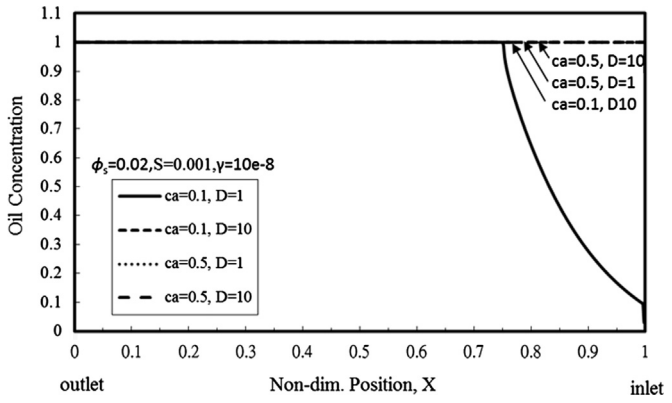


**Fig. 11.** Influences of droplet diameter and adhesion coefficient on oil concentration in work zone.

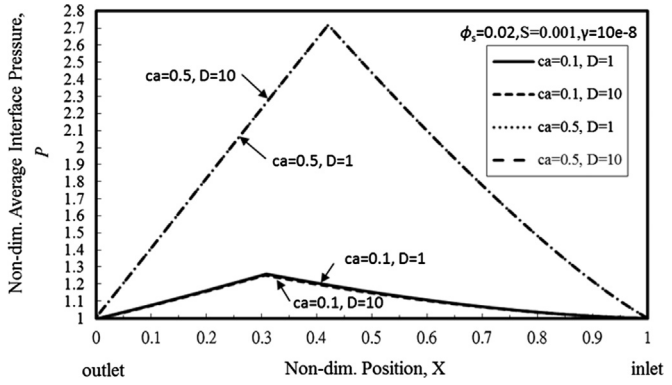


**Fig. 12.** Influences of droplet diameter and adhesion coefficient on average interface pressure in work zone.

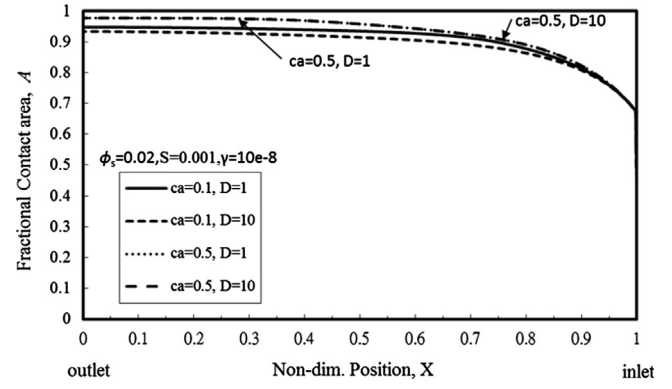


**Fig. 13.** Influences of droplet diameter and adhesion coefficient on fractional contact area in work zone.

## 5. Conclusion

An analysis combining the rheology of emulsion and plasticity of strip deformation has been developed for mixed lubricated strip rolling processes to understand the lubricity of oil-in-water emulsions. A double shooting numerical skill is used to find the adequate constant *C*, which is related to the lubricant flux, and the speed ratio *Z* defined as the strip speed at exit with respect to the roll speed. Some important findings are summarized as follows:

1. For lower dimensionless speed, the lubricant is not pressurized until it is very close to the roll bite where the oil droplet is trapped between the surfaces to form an oil column. This is the distinct pressuring zone presumed in the conventional Wilson's dynamic concentration model. On the contrary, the higher speed produces a smooth increase in hydrodynamic pressure from distant up stream and is basically not influenced by the supply oil concentration. While generally the higher speed yields the greater hydrodynamic pressure, its final value at the inlet-work boundary is lower than that of lower speed, due to the fact that more water is brought into the roll bite as the roll speed is enhanced. This is concordant with many experimental observations.
2. The O/W emulsion, though as low as 1–5% supply concentration, will eventually transform into the W/O state and become pure oil shortly before or after it enters the work zone. The hydrodynamic pressure thus rises swiftly to attain its climax and is able to offer tremendous lubrication function.
3. Neglecting the pressure increased in the far-end of the inlet zone and adopting the formulations of thin-film viscosities might underestimate the lubricant pressure.
4. In addition to the rolling speed, the asperity adhesion is the dominant factor to augment the hydrodynamic pressure and the oil concentration by confining the lubricant flux with smaller film thickness. The distribution of the average interface pressure on the roll and the asperity flattening on strip surface are mainly controlled by the adhesion coefficient in the mixed rolling process. The bigger oil droplet, which plays the secondary role, is also helpful to pressurize the lubricant.

## Acknowledgments

The authors wish to thank for the support from the National Science Council under Grant NSC99-2221-E-224-015-MY3.

## References

[1] Sheu S, Wilson WRD. Mixed lubrication of strip rolling. Tribology Transactions 1994;37:483–93.
[2] Wilson WRD, Chang D. Low speed mixed lubrication of bulk metal forming processes. Transactions of the ASME Journal of Tribology 1996;118:83–9.
[3] Chang D, Marsault N, Wilson WRD. Lubrication of strip rolling in the low-speed mixed regime. Tribology Transactions 1996;39:407–15.
[4] Lin H, Marsault N, Wilson WRD. A mixed lubrication model for cold strip rolling—Part 1: theoretical. Tribology Transactions 1998;41:317–26.
[5] Qiu ZL, Yuen WYD, Tieu AK. Mixed-film lubrication theory and tension effects on metal rolling processes. Transactions of the ASME Journal of Tribology 1999;121:908–15.
[6] Lu C, Tieu AK, Jiang Z. Modeling of the inlet zone in the mixed lubrication situation of cold rolling lubrication. Journal of Materials Processing Technology 2003;140:569–75.
[7] Nakahara T, Makino T, Kyogoku K. Observations of liquid droplet behavior and oil film formation in O/W type emulsion lubrication. Transactions of the ASME Journal of Tribology 1988;110:348–53.
[8] Zhu D, Biresaw G, Clark SJ, Kasun TJ. Elastohydrodynamic lubrication with O/W emulsion. Transactions of the ASME Journal of Tribology 1994;116:310–20.
[9] Yang H, Schmid SR, Reich RA, Kasun TJ. Elastohydrodynamic film thickness and tractions for oil-in-water emulsions. STLE Tribology Transactions 2004;47(1):123–9.
[10] Yang H, Schmid SR, Reich RA, Kasun TJ. Direct observations of emulsion flow in elastohydrodynamically lubricated contacts. ASME Journal of Tribology 2006;128:619–23.
[11] Cambiella A, Benito JM, Pazos C, Coca J, Ratoi M, Spikes HA. The effect of emulsifier concentration on the lubricating properties of oil-in-water emulsions. Tribology Letters 2006;22:53–65.
[12] Azushima A, Inagaki S, Ohta H. Plating out oil film thickness on roll and workpiece during cold rolling with O/W emulsion. Tribology Transactions 2011;54:283–9.
[13] Al-Sharif A, Chamniprasart K, Rajagopal KR, Szeri AZ. Lubrication with binary mixtures: liquid–liquid emulsion. Transactions of the ASME Journal of Tribology 1993;115:46–55.
[14] Wang SH, Szeri AZ, Rajagopal KR. Lubrication with emulsion in cold rolling. Transactions of the ASME Journal of Tribology 1993;115:523–31.

[15] Dai F, Khonsari MM. A theory of hydrodynamic lubrication involving the mixture of two fluids. Transactions of the ASME Journal of Applied Mechanics 1994;61:634–41.
[16] Szeri AZ, Wang SH. An elasto-plasto-hydrodynamic model of strip rolling with oil/water emulsion lubricant. Tribology International 2004;37:169–76.
[17] Yan S, Kuroda S. Lubrication with emulsion: first report, the extended Reynolds equation. Wear 1997;206:230–7.
[18] Yan S, Kuroda S. Lubrication with emulsion II. The viscosity coefficients of emulsions. Wear 1997;206:238–43.
[19] Wilson WRD, Sakaguchi Y, Schmid SR. A dynamic concentration model of lubrication with emulsions. Wear 1993;161:207–12.
[20] Wilson WRD, Sakaguchi Y, Schmid SR. A mixed flow model for lubrication with emulsions. STLE Tribology Transactions 1994;37(3):543–51.
[21] Cassarini S, Laugier M, Montmitonnet P. Modelling of metal forming lubrication by O/W emulsions. In: Lyngby N Bay (editor). 2nd international conference on tribology in manufacturing processes, ICTMP 2004. Nyborg, Denmark: DTU-IPL Publications; June 16–18th 2004. p. 713–20.
[22] Montmittonet P, Stephany A, Cassarini S, Ponthot JP, Laugier M, Legrand N. Modelling of metal forming lubrication by O/W emulsions. In: Proceedings of the 3rd international conference on tribology in manufacturing processes, ICTMP 2007. Yokohama, Japan; September 24–26 2007. p. 85–90.
[23] Kosasih PB, Tieu AK. Mixed film lubrication of strip rolling using O/W emulsions. Tribology International 2007;40:709–16.
[24] Tieu AK, Kosasih PB, Godbole A. A thermal analysis of strip-rolling in mixed-film lubrication with O/W emulsions. Tribology International 2006;39:1591–600.
[25] Benner JJ, Sadeghi F, Hoeprich MR, Frank MC. Lubricating properties of water in oil emulsions. Transactions of the ASME Journal of Tribology 2006;128:296–311.
[26] Lo SW, Yang TC, Cian YA, Huang KC. A model for lubrication by oil-in-water emulsions. Transactions of the ASME Journal of Tribology 2010;132:011801–9.